Multiphysics modelling and simulation of dry laser cleaning of micro-slots with particle contaminants

2012 J. Phys. D: Appl. Phys. 45 135401

(http://iopscience.iop.org/0022-3727/45/13/135401)

IOP PUBLISHING JOURNAL OF PHYSICS D: APPLIED PHYSICS

J. Phys. D: Appl. Phys. **45** (2012) 135401 (8pp) doi:10.1088/0022-3727/45/13/135401

Multiphysics modelling and simulation of dry laser cleaning of micro-slots with particle contaminants

Liyang Yue[1,3], **Zengbo Wang**[1,2,3] **and Lin Li**[1]

[1] Laser Processing Research Centre, School of Mechanical, Aerospace and Civil Engineering, University of Manchester, Sackville Street, Manchester, M13 9PL, UK
[2] Schools of Electronics Engineering, Bangor University, Dean Street, Bangor, Gwynedd, LL57 1UT, UK

E-mail: liyang.yue@postgrad.manchester.ac.uk and zengbo.wang@gmail.com

Received 7 December 2011, in final form 14 February 2012
Published 12 March 2012
Online at stacks.iop.org/JPhysD/45/135401

Abstract
Light could interact differently with thin-film contaminants and particle contaminates because of their different surface morphologies. In the case of dry laser cleaning of small transparent particles, it is well known that particles could function like mini-lenses, causing a localized near-field hot spot effect on the cleaning process. This paper looks into a special, yet important, phenomenon of dry laser cleaning of particles trapped in micro-sized slots. The effects of slot size, particle size and particle aggregate states in the cleaning process have been theoretically investigated, based on a coupled electromagnetic-thermal-mechanical multiphysics modelling and simulation approach. The study is important for the development and optimization of laser cleaning processes for contamination removal from cracks and slots.

(Some figures may appear in colour only in the online journal)

1. Introduction

Tiny particulate contaminants trapped in micro-slots and cracks are common residues in industrial manufacturing sectors [1], which are difficult to remove by conventional cleaning techniques such as chemical and ultrasonic cleaning. In a dry system, Van der Waals force predominates for tiny particles with a particle size less than a few micrometres and electrostatic force predominates for large particles, i.e. greater than about 50 μm in size [2]. Laser cleaning has been considered as a promising technology that is environmentally friendly. In dry laser cleaning, pulsed-laser irradiation generally causes rapid thermal expansion of substrate within a short time duration, which produces a strong lifting force that could overcome Van der Waals force and gravity to eject the contaminants away from the substrate surface [3, 4]. This method was first attempted for cleaning of tiny particles from solid surface by Tam and Zapka *et al* [5, 6]. It is noted that tiny transparent particle contaminants interact with laser light differently with thin-film contaminants, and it is well known that small transparent particle contaminants could manifest unique near-field effects such as lens focusing [7–9]. Previous researchers have experimentally quantified the influence of the near-field effect in dry laser cleaning system, and found it depended on factors of laser wavelength, substrate and particle properties [10, 11].

Meanwhile, the numerical simulation was employed to calculate the temperature gradient and distribution of energy intensity during the process of dry laser cleaning [12, 13]. Furthermore, Yang and Astratov verified the phenomena of regular attenuation of light intensity and alternate near-field focusing and defocusing effects in microspheres chain through experiments and software simulation [14]. However, until now there is no report in the literature on experiments or simulations about laser cleaning of a single particle or particle array trapped in micro-slot despite a number of publications about the particle–flat substrate system [15–17].

In this paper, a multiphysics numerical model is developed to simulate a micro-slot laser cleaning process. A commercial finite integral technique (FIT) software package—CST Microwave Studio 2011 (CST) was used in the study. The FIT method has been applied to solving problems in

[3] Authors to whom any correspondence should be addressed.

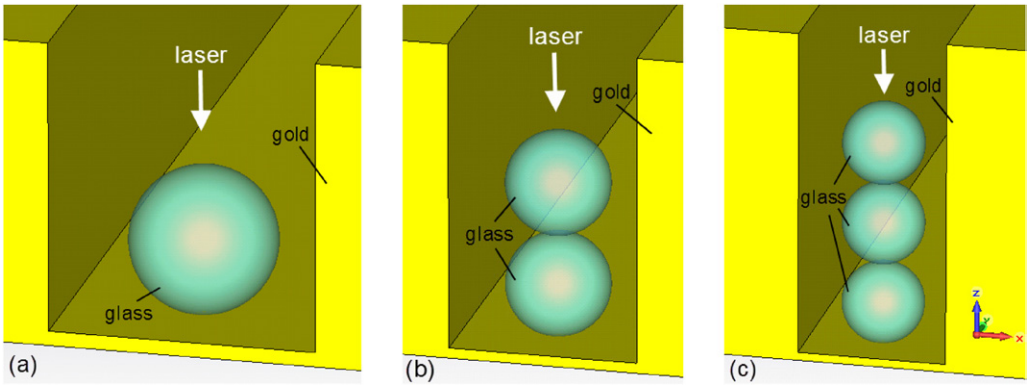

Figure 1. The geometric sketches of single (*a*), double (*b*) and triple (*c*) particle layouts for 1 μm diameter particle.

near-field optics previously. This method, proposed by Weiland, provides a universal spatial discretization scheme, applicable to various electromagnetic problems, ranging from static field calculations to high-frequency applications in time or frequency domain [18]. The electromagnetic intensity field distributions for varying slot widths and particle aggregate states were simulated and investigated relying on it. Laser energy flows, illustrated by Poynting vector field line plots [19], are presented to visualize and understand the near-field focusing effect inside the micro-slots. The electromagnetic simulation results were used as the heat source and fed into the thermal module in CST. Corresponding transient temperature field distributions were then obtained. From the CST temperature fields, the cleaning forces and cleaning threshold were determined following a well-known thermal-mechanical model.

2. Simulation process

2.1. Modelling geometry and materials

The particle contaminants are assumed to be spherical and transparent in this study. The model deals with both single and multiple particles sitting at the bottom of a micro-slot. The length of micro-slot (the y-axis direction) was considered as infinity. The width of slot (x-axis direction) varied from 1 to 5 μm and the depth of the slot (the z-axis direction) varies between 2 and 8 μm (leaving a one sphere gap from the top). Two sizes of particle (diameter 1 and 2 μm) were investigated in this research, and the geometric sketches of single, double and triple particle layouts for 1 μm diameter particle are shown in figures 1(*a*)–(*c*), respectively.

In the study, a metallic substrate (gold) and spherical glass micro-particles were selected as the representative modelling system, as gold is used in many aspects of semiconductor manufacturing, particularly in the assembly or packing processes, and glass particle is representative for transparent residue after various manufacturing processes [1, 20]. Corresponding thermal and optical properties of these materials at 248 nm wavelength laser are summarized in table 1 [21].

2.2. Laser source: temporal and spatial profile

The ultraviolet light irradiated by excimer laser provides higher emission current on the surface, which could enhance the cleaning effect [22]. For this reason, in this simulation, the laser source was considered to be linearly polarized (x-polarized) light irradiated by an excimer laser with rectangular flat top spatial profile, a wavelength of 248 nm and a pulse duration of 20 ns. The direction of beam was along the z-axis direction (top to down), as shown in figure 1. The typical spot size is about several square millimetres which covers the whole area of the modelled structure uniformly in the xy-plane. The typically temporal Gaussian pulse shape for an excimer laser was used in the study [23]:

$$I_0(t) = I_0 \left(\frac{t}{\tau_0}\right)^{\beta} \exp\left[\beta\left(1 - \frac{t}{\tau_0}\right)\right], \tag{1}$$

where $I_0(t)$, I_0 are the intensity of the incident beam at time t, and the peak intensity, respectively. The temporal shape factor is defined as $\beta = 1$, and pulse duration $\tau_0 = 20$ ns. As CST can only accept electric field amplitude $|E|$ as laser source input, the peak intensity value I_0 was converted to the amplitude of electric field E by [24]

$$|E| = \sqrt{\frac{2I_0}{cn\varepsilon_0}}, \tag{2}$$

where $c$is the speed of light in vacuum, n the refractive index of the medium (air in present case) and ε_0 the vacuum permittivity.

By considering that laser fluence (F_0) is related to peak intensity for a pulsed laser with [23]:

$$F_0 = I_0\tau_0 \tag{3}$$

and combining (2) and (3), gives

$$|E| = \sqrt{\frac{2F_0}{cn\varepsilon_0\tau_0}}, \tag{4}$$

which converts the laser fluence, often used by the laser processing community, to electric field amplitude $|E|$ used by the CST software.

Table 1. Optical and thermal properties of the substrate and the particles.

Materials	Density, ρ (kg m^{-3})	Thermal conductivity, k (W m^{-1} K^{-1})	Specific heat, C (J kg^{-1} K^{-1})	Refractive index, n	Extinction coefficient, k
Particle: glass	2330	1.3	700	1.51	0.000
Substrate: gold	19 300	318	130	1.484	1.636

2.3. Boundary conditions

Unlike most numerical methods, the basic idea of FIT is to apply the Maxwell's equation in integral form rather than the differential ones, which is given by [24]

$$\oiint_{\partial V} E \cdot \mathrm{d}A = \frac{Q(V)}{\varepsilon_0}, \tag{5}$$

$$\oiint_{\partial V} B \cdot \mathrm{d}A = 0, \tag{6}$$

$$\oint_{\partial S} E \cdot \mathrm{d}l = -\frac{\partial \Phi_s(B)}{\partial t}, \tag{7}$$

$$\oint_{\partial S} B \cdot \mathrm{d}l = \mu_0 \cdot I_s + \mu_0 \cdot \varepsilon_0 \cdot \frac{\partial \Phi_s(E)}{\partial t}, \tag{8}$$

where ∂V and V are its boundary surface and any three-dimensional volume, respectively, E is the electric field intensity, $\mathrm{d}A$ is the differential vector element of surface area A, $Q(V)$ is the net electric charge within the three-dimensional volume V, ε_0 is the permittivity of free space, B is the magnetic field density, ∂S and S are its boundary curve and any surface, respectively, $\mathrm{d}l$ is differential vector element of path length tangential to the path, $\partial/\partial t$ is the partial derivative with respect to time, $\Phi_s(B)$ and $\Phi_s(E)$ are the magnetic and electric flux through any surface S, respectively, μ_0 is the permeability of free space and I_s is the net electrical current passing through the surface S.

This change shows advantages due to high flexibility in geometric modelling and boundary handling as well as incorporation of arbitrary material distributions and material properties such as anisotropy, non-linearity and dispersion. To obtain better accuracy on solver Cartesian grids are employed to the current model [25]. Meanwhile, due to the fact that the software is only capable of handling finite size structures, the boundary conditions on the edge of model were defined as open boundary in both electric and thermal modules. The open boundary condition mimics the situation that materials at the computing boundaries extend themselves to the infinite space.

3. Results and discussion

3.1. Electromagnetic modelling: intensity fields in micro-slots

Figure 2(*a*) shows the normalized enhancement factor of intensity fields, defined as z-component of time-averaged Poynting vector $I = Re(S_z)$, at the contacting point (Point A as in insets) of particle and substrate for single, double and triple layers of microspheres (diameter $d = 1.0\,\mu$m) located inside different size micro-slots (width $1 < S < 5\,\mu$m). It can be seen that, regardless of the slot width, single layer particles produce a much stronger focus at the slot bottom surface than those by both the double and triple layers, and triple layers show a stronger focus than double layers. The slot width (S) has clear influences on the focusing fields. For a single layer (1P), intensity enhancement at the focal point is weak at narrow slot widths $1\,\mu\mathrm{m} < S < 1.4\,\mu\mathrm{m}$. The intensity enhancement was boosted at slot width $1.4\,\mu\mathrm{m} < S < 3\,\mu\mathrm{m}$ with a resonance peak of 32 times of the incoming beam intensity forming at $S = 1.8\,\mu$m and stabilized to about 26.6 (mean value) with a weak oscillation at slot width $S > 3\,\mu$m. A similar tendency was observed for double layers (2P), with the intensity peak increasing at the slot width $S = 2.2\,\mu$m, and being stabilized to about 7 at slot widths $S > 3\,\mu$m. For the three layer particles (3P), more oscillations were seen within the investigated slot width range. The field intensity peak appeared at the slot width around $S = 2.6\,\mu$m. To illustrate the field focusing effects at resonance peaks (P1, P2, P3), the corresponding 2D field distributions in both *XZ*-planes (across particle centre) and *XY*-planes (across point A) are presented in figures 2(*b*)–(*g*).

Similar to figure 2, figure 3 shows the results of electromagnetic simulation with exactly the same modelling settings and parameters except that the particle diameter was increased from 1 to 2 μm. The single layer particle of 2 μm diameter sphere (figure 3(*a*)) behaves similarly to a single 1 μm diameter sphere (figure 2(*a*)) with the main field enhancement within the slot width $2.4\,\mu\mathrm{m} < S < 3.6\,\mu\mathrm{m}$. However, it should be emphasized that the near-field focusing effect of single particle layout for the 2 μm particle is much stronger than the 1 μm particle. The intensity for 2 μm particle is always above 30 with a maximum of 63.44 for the slot width $S = 3\,\mu$m (P1 in figure 3(*a*)). The curve stabilizes to around 40 at the end. For the double and triple layered particles, the graphs show peaks at $S = 3.8\,\mu$m and $S = 3.2\,\mu$m and gradually stabilize to about 5 and 3, respectively, along with the increase in the slot width. It is found that the stabilized values of double and triple layered 2 μm particles are lower than those for 1 μm particles, as shown in figures 2(*a*) and 3(*a*).

From figures 2(*b*) and 3(*b*), it is clear that the focusing point of single particle layout, which has the highest electric field intensity in the three layouts, is close to the substrate. Also, from figures 2(*c*) and 3(*c*), it can be seen that the highest intensity concentrates at the centre of the slot bottom, which forms the central highest peak, and the height of secondary peaks was found to be lower for the same size particle. These two aspects mean that a better near-field focusing effect was obtained in the single particle layout, which benefits laser cleaning and most of the material processing (micro/nano fabrication) applications [26, 27]. Conversely , the strongest focusing positions of both double and triple particle layout are

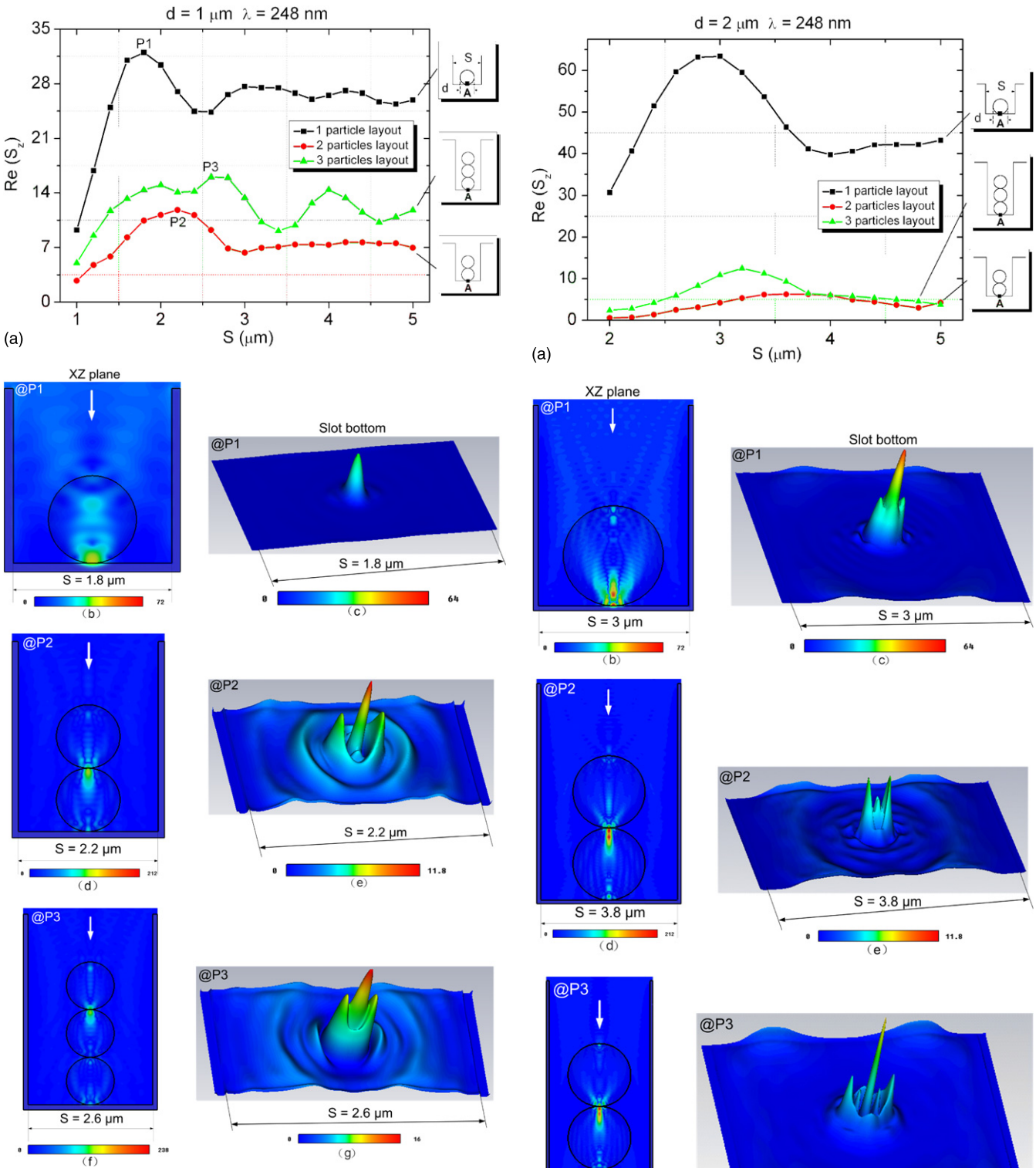

Figure 2. (*a*) Peak intensity on substrate surface beneath 1 μm diameter particles as a function of slot width. (*b*)–(*g*) Corresponding 2D cross-sectional views of the maximum intensity fields in the *XZ*-plane (*b*), (*d*), (*f*) and *XY*-plane (*c*), (*e*), (*g*) for single (P1), double (P2) and triple (P3) layered particles.

Figure 3. (*a*) Peak intensity on the substrate surface beneath the 2 μm diameter particles as a function of slot width. (*b*)–(*g*) Corresponding to the 2D cross-sectional views of the maximum intensity fields in the *XZ*-plane (*b*), (*d*), (*f*) and *XY*-plane (*c*), (*e*), (*g*) for single (P1), double (P2) and triple (P3) layered particles.

at the contact point of the first and second particles counting from the top, as shown in figures 2(*d*), (*f*) and 3(*d*), (*f*), which are far from the substrate. In addition, the phenomenon of multiple secondary peaks or double highest peaks was

observed on the intensity field in the *XY* plane for the cases of double and triple particle layouts. The light energy is not entirely focused to the position under the particles. Instead, it decentralizes and spreads in certain areas. The phenomenon is considered to be caused by the interference of particle array and Newton's rings effect [28]. For this reason it would be difficult for the substrate to absorb the focusing energy through the spheres in the multiple particle situations, supported by the fact that the energy intensity values for the multiple particle layouts are much lower than for the single particle layout, as shown in figures 2(*a*) and 3(*a*). However, by observing distributions shown in figures 2(*d*), (*f*) and 3(*d*), (*f*), the substrate under the multiple particle layout may still be heated, but the cleaning effect would be weakened. It also demonstrates that the distribution of intensity and the full width at half maximum (FWHM) of the beam on the substrate can be controlled using different particle arrays, which could be useful for laser patterning applications. Figure 3(*b*) illustrates that the focusing range of 2 μm diameter particle is much wider than that of the 1 μm diameter one, and more light waves penetrate through the single particle layout, which results in a higher magnitude of intensity in figure 3(*a*). On the other hand, based on the established literature [14], it is known that light intensity attenuates through microsphere chain. And a larger particle accelerates the defocusing propagation and intensity attenuation in it, which could explain the fact that higher magnitude of intensity is observed on the slot bottom in figures 2(*e*), (*g*) compared with those in figures 3(*e*), (*g*).

A special phenomenon observed in the multiple particle layouts is that the near-field focusing and defocusing are alternating, with even number of particles producing a defocusing effect and odd number of particles giving a focusing effect at the bottom of the sphere. For the same size particles, the focusing effect initiated by an odd number of particles provides higher magnitude of intensity and energy level on the slot bottom compared with the defocusing effect of an even number of particles, as shown in figures 2(*a*) and 3(*a*). This phenomenon seems to be independent of the slot width. Generally, for the single particle layout the near-field focusing effect is the only optical interaction for this material and the sphere size and the focal position is at the bottom of the sphere. In the two particle layout, it is possible for the defocusing effect to happen at the bottom sphere. The defocusing effect is due to the fact that the light focused by the top sphere starts to disperse through the bottom sphere. When the third particle was added into the particle array, the light was focused to the substrate again through the third particle, despite the attenuation of intensity during the propagation. This phenomenon was also observed experimentally by Yang and Astratov [14].

3.2. Electromagnetic modelling: energy flow visualization

To understand the influence of the slot width on the distribution of Poynting vector, the power flow of the single 1 μm diameter particle layout is presented in figure 4. From figure 4(*a*) (slot width equals the diameter of the sphere), it can be noticed that there are four singular points located in the centre of the sphere. The phase trajectories in the vicinity of the singular

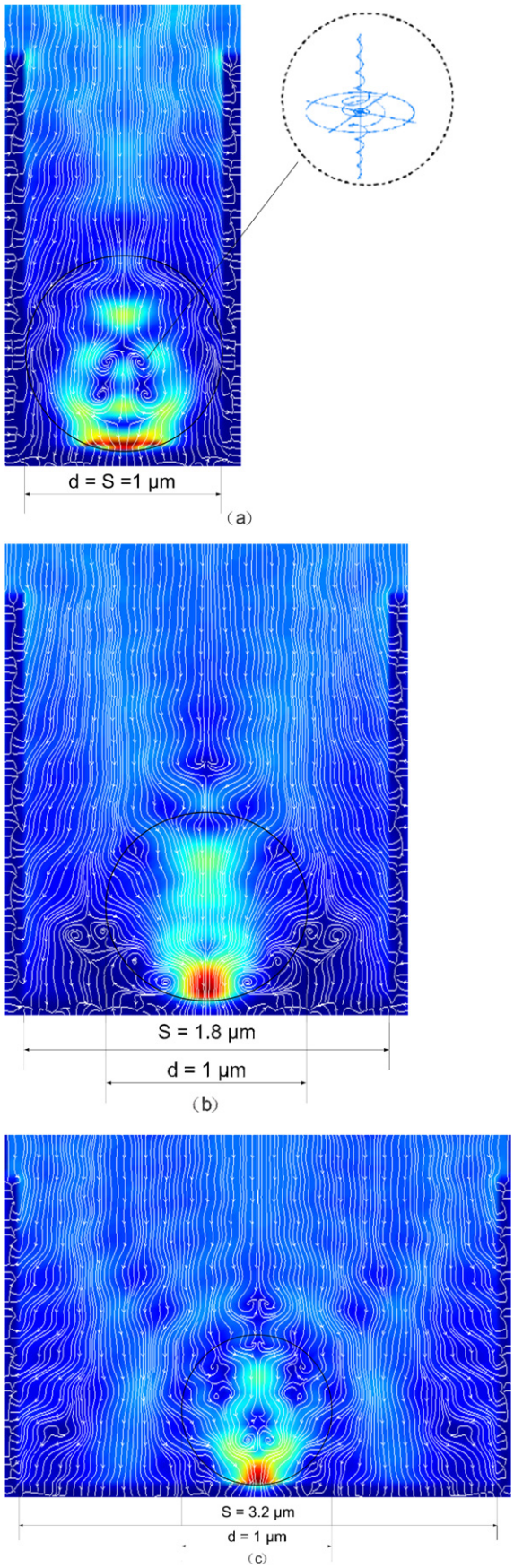

Figure 4. The energy flow field lines of single 1 μm diameter particle in slot (*a*) at slot width = 1 μm (*b*) slot width = 1.8 μm (*c*) slot width = 3.2 μm. The schematic of 3D vortex coupling energy into different planes is shown as inset in (*a*).

points form the clockwise vortexes which are in the relatively low electric intensity areas. It is known that, phase trajectories of the system contain one and a half degree of freedom in the vicinity of singular points, and related clockwise vortex shape represents a stable focus in the phase space [29]. Also, power flow couples to the other planes through these singular points [30]. The inset in figure 4(*a*) illustrates the typical helical trajectories that 3D vortex couples energy into different planes. When the slot width is increased to 1.8 μm (figure 4(*b*)), the sphere has enough space to absorb more light than its diameter resulting in the intensity of electric field and the magnitude of Poynting vector on the substrate to be higher than for smaller slot dimensions. Due to the reflection or inference of light on the side walls, vortex trajectories and corresponding low intensity areas move closer to the sphere's lower boundary as shown in figure 4(*b*). When the slot width increases to above 3 μm, the intensity on the substrate under the sphere approaches to a constant value as shown in figure 2(*a*). In spite of changing positions of vortex to the upper part of the sphere, the sphere in a 3.2 μm wide slot still collects light from spaces wider than its diameter. As a result the intensity on substrate under the sphere is higher than that in the case of 1 μm slot width.

It can be summarized that the envelope of the light energy entering the particle is a limiting factor for the intensity at the bottom of the sphere, which could be wider than the diameter of the particle. The light intensity attenuates and couples to other phase planes through the vortex trajectories. When the vortex trajectories move to the sphere's lower boundary, electric intensity and corresponding magnitude of Poynting vector on the substrate is raised because of the sphere focusing effect.

3.3. Electromagnetic to thermal modelling: temperature fields

In this work, the electromagnetic field data were coupled to the thermal field for the analysis of temperature distributions. In this modelling, the laser fluence (0.2 J cm^{-2}) and related temporal pulse shape (Gaussian pulse) and pulse lengths of 20 ns are loaded. Figure 5(*a*) shows the temporal temperature distribution on the substrate surface under the sphere for single-, two- and three-particle layouts of 1 μm diameter particle at widths corresponding to P1, P2 and P3 in figure 2(*a*), respectively. From figure 5(*a*), it is found that the substrate temperature of the single-particle layout is normally higher than those in the other two cases, which corresponds to the result of electromagnetic simulation. The higher magnitude of intensity on the slot bottom creates stronger substrate heating, and a peak temperature of 1928 K is achieved at 10 ns on the substrate. Also, due to the re-focusing effect of the third particle (shown in figure 2(*f*)), the peak substrate temperature of the three-particle layout (1462 K) is higher than for the two-particle layout (1081 K). However, the peak temperatures of all three layouts are achieved at 10 ns and the temperature on the substrate returns to room temperature after 18 ns. The melting point of the gold substrate is 1337 K [21]. Therefore a laser beam with a fluence of 0.2 J cm^{-2} could damage the substrate

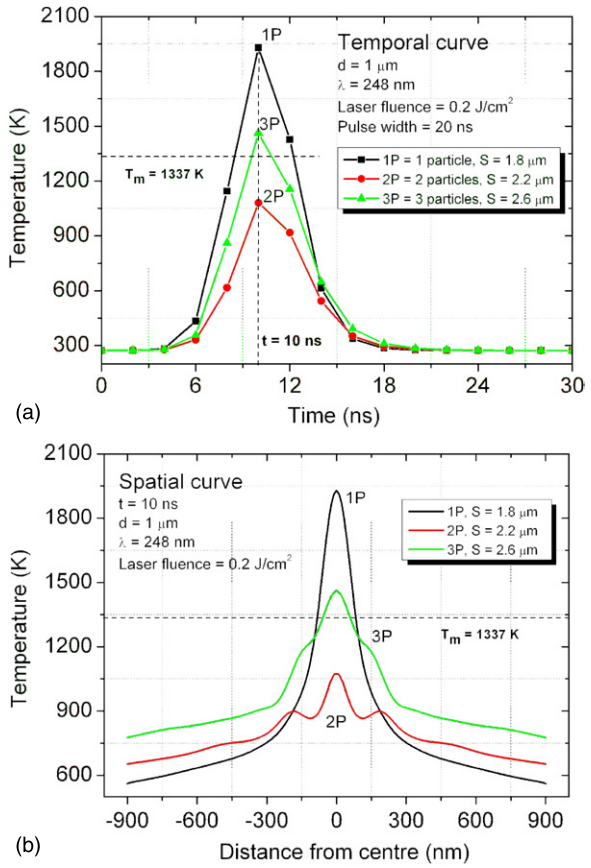

Figure 5. (*a*) Temporal temperature distribution of the substrate surface under single, double and triple particles at optimized slot widths (*b*), corresponding to spatial temperature distribution of substrate surface at $t = 10$ ns.

in single- and three-particle layouts, but may be suitable for the two-particle layout cleaning. For laser cleaning, a much lower fluence would be needed for the single- and three-particle layouts.

Figure 5(*b*) describes the spatial temperature distribution of substrate along the x-axis of single-, two- and three-particle layouts at 10 ns (peak temperature time). The curve of the one-particle layout is nearly Gaussian distribution in shape. However, the curves of two- and three-particle layouts do not form a typical Gaussian distribution because of interference of particle array and Newton's rings phenomenon, though they have obvious peaks in the centre.

3.4. Thermal to mechanical modelling: cleaning thresholds

Due to the short pulse laser irradiation, there is a rapidly increasing temperature gradient on the substrate. This sudden increase in temperature generates a cleaning force which ejects particles from the substrate surface. The equation of dry laser cleaning force per unit area, f_1, is given by [31]

$$f_1 = \gamma E_s \Delta T(0, t) \tag{9}$$

where γ and E_s are the linear thermal expansion coefficient and the elastic modulus of the substrate, respectively. $\Delta T(0, t)$ is the temperature rise at the substrate surface and time t,

which is given by $\Delta T(0,t) = T(0,t) - T_0$, where T_0 is the initial temperature at substrate surface. In this study, $\Delta T(0,t)$ initiated by multiple laser fluences is calculated by the thermal module in CST 2011. The cleaning force can be obtained by calculating the contact area between particle and substrate, which relates to the dominant adhesion force—Van der Waals force, F_v, which is expressed by the following equations [2]:

$$F_v = \frac{hr}{8\pi z^2}, \tag{10}$$

where, r, h and z are the particle radius, the material-dependent Liftshitz–Van der Waals constant and the atomic separation between the particle and surface, respectively. Assuming Van der Waals force is the main adhesion force applied to the particle, radius of contact area, a, and elastic depth, d, are deduced by the following equations [22]:

$$F_v = \tfrac{4}{3}E^* r^{1/2} d^{3/2}, \tag{11}$$

$$a = \sqrt{rd}, \tag{12}$$

where E^* is the elastic modulus of two bodies, which is given by

$$\frac{1}{E^*} = \frac{1-v_1^2}{E_1} + \frac{1-v_2^2}{E_2}, \tag{13}$$

Where E_1, E_2 and v_1, v_2 are the elastic modulus and Poisson's ratios associated with each part, respectively. Thus, the cleaning force initiated by laser, F_c, is expressed by the following equation:

$$F_c = f_1 \pi a^2. \tag{14}$$

Its direction is opposite to the Van der Waals force and gravity of particles. For removal of the tiny particles in micro-slot the cleaning force, F_c, must be larger than the main adhesion force—Van der Waals force, F_v, which is millions of times larger than gravity of particle by calculation. For this reason, it is found that the number of particles in the layout is only able to influence the gravity of the particles' chain, whose effect on the adhesion force is extremely restricted. Conversely, the size of particles (particle radius, r) controls the magnitude of dominant adhesion force—Van der Waals force by equation (10). For obtaining preconditions of cleaning, $F_c > F_v$, related cleaning force generated from laser also depends on it. Therefore, the cleaning threshold in this study is the minimum input laser energy density required to generate enough cleaning force to overcome Van der Waals force and eject the particles from the surface. The damage threshold is defined as the minimum input laser energy to cause surface damage. The damage in this study is assumed to be only caused by thermal reason. The complicated mutual surface stresses between particle and substrate are ignored in the model. In this case, the surface temperature should not be above the melting point of the substrate. If it is, the surface is considered as damaged and not allowed.

Based on the above equations and the numerical model, the cleaning and damage thresholds for 1 μm and 2 μm diameter particles under different layouts are presented in tables 2 and 3, respectively. The values of Van der Waals force used for tables 2 and 3 are 0.179×10^{-6} N and 0.359×10^{-6} N, respectively. It is shown that for the single-particle layout the cleaning and damage thresholds for the 1 μm diameter particle (table 2) are obviously higher than those for 2 μm diameter particle (table 3) due to the relatively weaker near-field focusing effect and corresponding temperature rise. However, for the double- and triple-particle layouts the cleaning and damage thresholds for the 1 μm diameter particle (table 2) are lower than for 2 μm diameter particle (table 3), which is caused by the fact that 2 μm diameter particle provides the stronger defocusing effect and the light intensity gradually attenuates and becomes weak on the substrate. Meanwhile, it is realized that for the same size particles the cleaning and damage thresholds of single- and triple-particle layouts are lower than for the two-particle layout, which corresponds to the simulation results of electromagnetic fields, as shown in figures 2(*a*) and 3(*a*). It proves that the near-field focusing effect initiated by various particle layouts plays a very important role in the dry laser cleaning system, which needs to be concerned with the measurement of cleaning and damage thresholds. Finally, it is worth mentioning that optical near-fields could be strongly influenced by the factors such as particle shape, transparency, substrate material [10, 32, 33], and it would be interesting to study non-spherical or nano-transparent contaminants trapped in micro-slots in the future work.

Table 2. Cleaning and damage threshold for the 1 μm diameter glass particles in gold micro-slot.

Thresholds	Single-particle layout	Double-particle layout	Triple-particle layout
Cleaning threshold (mJ cm^{-2})	42.0	93.3	63.4
Damage threshold (mJ cm^{-2})	126.9	263.4	179.0

Table 3. Cleaning and damage thresholds for the 2 μm diameter glass particles in gold micro-slot.

Thresholds	Single-particle layout	Double-particle layout	Triple-particle layout
Cleaning threshold (mJ cm^{-2})	17.4	176.5	87.9
Damage threshold (mJ cm^{-2})	61.8	626.1	311.7

Note: Cleaning threshold is the minimum input laser energy density required to generate enough force to eject the particles from the surface. *Damage threshold* is the minimum input laser energy to cause surface damage.

4. Conclusions

We have explored the fundamental physics behind dry laser cleaning of particle contaminants trapped in micro-slots. The multiphysics electromagnetic-thermal-mechanical coupled numerical models have revealed several important

physical effects. The magnitudes of field intensity on substrate in certain range of slot width could be elevated by about 25% for 1 and 2 μm diameter particles, and their energy distributions on the slot bottom were influenced by particle layouts. The transparent spheres could induce the formation of vortex phase trajectories on the laser flow lines, and partial laser power could couple to the other planes of media through these singular points, which affects the focusing effect of the particle. The coupled temperature field calculation has revealed enhanced temporal and spatial heating scenario of the substrate beneath different particle layouts, and corresponding surface cleaning and damage thresholds were finally determined.

References

[1] Lee Y P, Lu Y F, Chan D S H, Low T S and Zhou M S 1998 Steam laser cleaning of plasma-etch-induced polymers from via holes *Japan. J. Appl. Phys.* **37** 2524–9

[2] Mittal K L 1988 *Particles on Surfaces* vol 1 (New York: Plenum) pp 3–400

[3] Lu Y F, Sung W and Hong M 1996 Laser removal of particles from magnetic head sliders *J. Appl. Phys.* **80** 499–504

[4] Lu Y F, Takai M and Komuro S 1994 Surface cleaning of metals by pulsed-laser irradiation in air *Appl. Phys.* A **59** 281–8

[5] Tam A C, Leung W P, Zapka W and Ziemlich W 1992 Laser cleaning techniques for removal of surface particulates *J. Appl. Phys.* **71** 3515–23

[6] Zapka W, Ziemlich W and Tam A C 1991 Efficient pulsed laser removal of 0.2 μm sized particles from a solid surface *Appl. Phys. Lett.* **58** 2217–9

[7] Wang Z B, Guo W, Li L, Luk'yanchuk B, Khan A, Liu Z, Chen Z C and Hong M H 2011 Optical virtual imaging at 50 nm lateral resolution with a white-light nanoscope *Nature Commun.* **2** 218

[8] Taubner T, Korobkin D, Urzhumov Y, Shvets G and Hillenbrand R 2006 Near-field microscopy through a SiC superlens *Science* **313** 1595

[9] Bohren C F and Huffman D R 1983 *Absorption and Scattering of Light by Small Particles.* (New York: Wiley) p 7

[10] Zheng Y W, Luk'yanchuk B S, Lu Y F, Song W D and Mai Z H 2001 Dry laser cleaning of particles from solid substrates: experiments and theory *J. Appl. Phys.* **90** 2135

[11] Luk'yanchuk B S, Zhang Y W and Lu Y F 2000 Laser cleaning of solid surface: optical resonance and near-field effects *Proc. SPIE* **4065** 576

[12] Lu Y F, Song W D, Ye K D, Hong M H, Liu D M, Chan D S H and Low T S 1997 Removal of submicron particles from nickel-phosphorus surfaces by pulsed laser irradiation *Appl. Surf. Sci.* **120** 317–22

[13] Oh B, Lee J W, Lee J M and Kim D 2008 Numerical simulation of laser shock cleaning process for micro-scale particle removal *J. Adhes. Sci. Technol.* **22** 635–50

[14] Yang S and Astratov V N 2008 Photonic nanojet-induced modes in chains of size-disordered microspheres with an attenuation of only 0.08 dB per sphere *Appl. Phys. Lett.* **92** 261111

[15] Mosbacher M, Munzer H J, Zimmermann J, Solis J, Boneberg J and Leiderer P 2001 Optical field enhancement effects in laser-assisted particle removal *Appl. Phys.* A **72** 41–4

[16] Halfpenny D R and Kane D M 1999 A quantitative analysis of single pulse ultraviolet dry laser cleaning *J. Appl. Phys.* **86** 6641

[17] Mosbacher M, Chaoui N, Siegel J, Dobler V, Solis J, Boneberg J, Afonso C N and Leiderer P 1999 A comparison of ns and ps steam laser cleaning of Si surfaces *Appl. Phys.* A **69** S331–4

[18] Weiland T 1996 Time Domain Electromagnetic Field Computation with Finite Difference Methods *Inter. J. Numer. Modelling* **9** 295–319

[19] Belcher J W and Olbert S 2003 Field line motion in classical electromagnetism *Am. J. Phys.* **71** 220

[20] Magagnin L, Maboudian R and Carraro C 2002 Gold deposition by galvanic displacement on semiconductor surfaces: effect of substrate on adhesion *J. Phys. Chem.* B **106** 401–7

[21] Chase M W 1998 *NIST-JANAF Thermo-Chemical Tables* 4th edn (USA: The American Chemical Society and the American Institute of Physics) pp 1881–7

[22] Luk'yanchuk B S 2002 *Laser Cleaning* (Singapore: World Scientific) pp 148–430

[23] Bauerle D 2000 *Laser Processing and Chemistry* (Beilin: Springer) pp 105–20

[24] Reitz J R and Frederick J M 1960 *Foundations of Electromagnetic Theory* (England: Addison-Wesley) pp 25–304

[25] Wang Z B, Guo W, Luk'yanchuk B S, Whitehead D J, Li L and Liu Z 2008 Optical near-field interaction between neighbouring micro/nano-particles *J. Laser Micro/Nanoeng.* **3** 14–8

[26] Khan A, Wang Z B, Sheikh M A, Whitehead D J and Li L 2010 Parallel near-field optical micro/nanopatterning on curved surfaces by transported micro-particle lens arrays *J. Phys. D: Appl. Phys.* **43** 305302

[27] Khan A, Wang Z B, Sheikh M A, Whitehead D J and Li L 2011 Laser micro/nano patterning of hydrophobic surface by contact particle lens array *Appl. Surf. Sci.* **258** 774–9

[28] Lipson A, Lipson S G and Lipson H 2010 *Optical Physics* 4th edn (Cambridge: Cambridge University Press) p 559

[29] Karlov N V, Kirchenko N A and Luk'yanchuk B S 2000 *Laser Thermochemistry: Fundamentals and Applications* (Cambridge: Cambridge International Science Publishin) pp 54–9

[30] Wang Z B, Luk'yanchuk B S, Hong M H, Lin Y and Chong T C 2004 Energy flow around a small particle investigated by classical Mie theory *Phys. Rev.* B **70** 035418

[31] Lu Y F, Song W D, Zhang Y and Low T S 1998 Theoretical model and experimental study for dry and steam laser cleaning *Proc. SPIE—Int. Soc. Opt. Eng* **3550** 7–18

[32] Nieminen T A, Rubinsztein-Dunlop H and Heckenberg N R 2001 Calculation and optical measurement of laser trapping forces on non-spherical particles *J. Quant. Spectrosc. Radiat. Transfer.* **70** 627–37

[33] Xie C G and Li Y Q 2002 Raman spectra and optical trapping of highly refractive and nontransparent particles *Appl. Phys. Lett.* **81** 951–3